MNRAS **000**, 1–6 (2018) Preprint 16 September 2019 Compiled using MNRAS LATEX style file v3.0

Photometric Selection of Red Clump Stars with a Mixed Density Network

Madeline Lucey[1⋆], Yuan-Sen Ting[2,3,4], Nesar Ramachandra[5], Keith Hawkins[1]
[1] *Department of Astronomy, the University of Texas at Austin, 2515 Speedway Boulevard, Austin, TX 78712, USA*
[2] *Institute for Advanced Study, Princeton, NJ 08540, USA*
[3] *Department of Astrophysical Sciences, Princeton University, Princeton, NJ 08544, USA*
[4] *Observatories of the Carnegie Institution of Washington, 813 Santa Barbara Street, Pasadena, CA 91101, USA*
[5] *High Energy Physics Division, Argonne National Laboratory, Lemont, IL 60439, USA*

Accepted .... Received ...; in original form ...

ABSTRACT
Large pristine samples of red clump stars are highly sought after given their ability to give precise distances even at large distances. However, it is difficult to cleanly select red clumps stars because they can have the same $T_{\rm eff}$ and log g as red giant branch stars which are not standard candles. Recently, it was shown that the asteroseismic parameters ΔP and $\Delta\nu$ which are used to accurately select red clump stars can be derived from spectra. In this study, we use a mixed density network to derive the ΔP,$\Delta\nu$, $T_{\rm eff}$and log $g$from photometry in order to select a clean sample of red clump stars. We combine data from 2MASS, AllWISE, *Gaia*, and Pan-STARRS to create a 13-band SED along with parallax information. We achieve a contamination rate of $\sim$25%. We then use this catalog to make a precise map of the distant Galaxy. In the process of creating the red clump catalog we also create a giant stars catalog, which will both be available to the public.

Key words: stars: distances, Galaxy:structure

1 INTRODUCTION

Distances are one of the most important and yet hardest measurements to make in astronomy. The *Gaia* Mission aims to provide parallax measurements for billions of stars in order to produce a map of the Galaxy (Gaia Collaboration et al. 2016). However, the *Gaia* mission will be plagued with large errors in the distance Galaxy as the error on distance derived from parallax goes as distance squared. Standard candles, such as red clump (RC) stars, where the distance is derived using the distance modulus have errors that are linear with distance. For example, with high precision photometry, RC stars can provide distances with errors $\sim$ 6% at distances up to $\sim$ 10 kpc (Bovy et al. 2014; Hawkins et al. 2017). Therefore, standard candles can provide more precise distances for objects in the distant Galaxy than parallaxes and are an excellent complement to the *Gaia* catalog.

RC stars have been used as standard candles since the late nineties (Stanek et al. 1997, 1998). RC stars are burning helium in their core and also have a hydrogen burning shell. These two components are thought to balance so that the luminosity of the star has very weak dependence on mass and metallicity (Castellani et al. 1992). However, selecting a pristine sample of red clump stars can be difficult. Red giant branch (RGB) stars have inert Helium cores with a hydrogen burning shell but can have the same $T_{\rm eff}$ and log g as RC stars.

Asteroseismology has proven to be the most accurate method for selecting red clump stars (Bedding et al. 2011; Mosser et al. 2011; Stello et al. 2013; Mosser et al. 2014). The average large frequency spacing ($\Delta\nu$) goes as the square root of the mean stellar density (Chaplin & Miglio 2013). It has been shown that the distribution of $\Delta\nu$ values for RGB and RC stars are distinct (Miglio et al. 2009; Mosser et al. 2010). RC stars are more constrained in this space with $\Delta\nu < 5$ μHz. While, RGB stars can have $\Delta\nu > 20$ μHz. Red giant stars have been shown to have coupling between the gravity waves in the dense radiative core and the acoustic waves in the envelope (Beck et al. 2011). RC and RGB clearly separate in the period spacing (ΔP) of these mixed modes with RC stars typically having ΔP > 200s and RGB stars having ΔP <100s (Bedding et al. 2011; Mosser et al. 2011; Stello et al. 2013; Mosser et al. 2014). However, ΔP is a difficult measurement and has only been measured for a fraction of the *Kepler* and CoRoT samples (Girardi 2016).

Recently, Hawkins et al. (2018) showed the ΔP and the $\Delta\nu$ spacing can be inferred from a stellar spectrum. It has long been thought that the carbon to nitrogen ratio, [C/N],

⋆ E-mail: m_lucey@utexas.edu

would be different in RC stars relative to RGB stars because of mixing that occurs along the upper RGB phase (Martell et al. 2008; Masseron & Gilmore 2015; Masseron & Hawkins 2017; Masseron et al. 2017). Using *The Cannon* (Ness et al. 2015; Casey et al. 2016), Hawkins et al. (2018) showed the carbon and nitrogen bands in spectra from the Apache Point Observatory Galactic Evolution Experiment (APOGEE) (Majewski et al. 2015) survey can be used to infer the ΔP and $\Delta\nu$ and therefore, used to select RC stars. Building off of this work, Ting et al. (2018) presents a catalog of $\sim$ 100,000 RC stars from the APOGEE and LAMOST catalogs (Xiang et al. 2017). However, $>$ 70% of that sample is within 3 kpc of the Sun where *Gaia* gives more precise distances (Ting et al. 2018). This represents the largest constraint to recent spectroscopic surveys. Spectra require more flux than photometry and therefore high signal-to-noise (S/N) data can only be achieved nearby.

In this work we aim to make use of the vast amount of available photometry to obtain the largest and most distant sample of red clump stars yet. It is reasonable to assume that if the information to accurately select red clump stars is in the spectra, then the same information is the the spectral energy distribution (SED) just with a much weaker signal. In Section 2 we describe the photometry selection we use to create the SED. In Section 3, we describe the innovative method we develop to infer the $T_{\rm eff}$, log g, ΔP and $\Delta\nu$from the SEDs and how we use those parameters to select a sample of RC stars. Finally, in Section 4 we present a map of the Milky Way made with our selection of red clump stars and discuss the results.

2 DATA

2.1 Photometry

In this work we make use of data from *Gaia* DR2 (Gaia Collaboration et al. 2018), Pan-STARRS1 (Chambers et al. 2016), 2MASS (Skrutskie et al. 2006) and AllWISE (Wright et al. 2010; Mainzer et al. 2011) photometric catalogs, along with *Gaia* DR2 parallaxes. We include all the pass bands from *Gaia* (G, BP, RP), Pan-STARRS (g,r,i,z,y) and 2MASS (J, H, K_S). We use only the two bluest AllWISE bands, W1 and W2. The two other bands, W3 and W4, are shallower, have lower spatial resolution and do not contain much additional information about the SED of red clump stars. We also make use of the provided *Gaia* DR2 crossmatches with Pan-STARRS1, 2MASS, and AllWISE which take into account the motions of the targets and the varying epochs of the different surveys (Marrese et al. 2019).

We perform multiple quality cuts to ensure we only use accurate photometry and parallaxes. As recommended by Arenou et al. (2018) and Evans et al. (2018) to ensure quality *Gaia* DR2 photometry we applying the following cut:

$1.0+0.015(\mathrm{BP}-\mathrm{RP})^2 <$ phot_bp_rp_excess_factor$<$ $1.3 + 0.060(\mathrm{BP}-\mathrm{RP})^2$

We also apply a quality cut using the renormalised unit weight error (ruwe<1.4) to ensure quality parallax measurements. Last, we only use “A” quality photometry from 2MASS and AllWISE.

2.2 Training and Testing Data

In order to train the network and evaluate our method we require a set of data with known asteroseismic parameters. We use the catalog presented in Ting et al. (2018) which provides ΔP and $\Delta\nu$ measurements for LAMOST DR3 (Xiang et al. 2017) spectra within a convex hull of red clump $T_{\rm eff}$ and log g values (see Figure 4). This catalog is derived using a data-driven neural network which finds a mapping between the pixel values of the spectra to ΔP and $\Delta\nu$. For our training we include only high quality ΔP and $\Delta\nu$ measurements from this catalog, requiring the spectra to have $S/N_{\rm pix}$ >75. With this quality cut, the training sample has a contamination rate of $\sim$3%. We train our ΔP and $\Delta\nu$ network on a subset of 30,000 stars from this sample. We include data with $S/N_{\rm pix}$ <75 in our testing set of 100,000 of stars to determine the accuracy of our inference on lower S/N data.

In addition to this training set we require another training set to determine photometric $T_{\rm eff}$ and log g outside of the convex hull. For this, we use the LAMOST DR3 stellar catalog. Here, we require the training set of 200,000 to have g-band S/N >50. Again, out testing set of 900,000 stars does not have a S/N cut.

With both training sets we perform a sky crossmatch with *Gaia* DR2 using TOPCAT (Taylor 2005). We then use the provided *Gaia* DR2 crossmatches to obtain the photometry from AllWISE, 2MASS, and Pan-STARRS1.

3 METHOD

3.1 Mixed Density Network

In this work, we infer the ΔP, $T_{\rm eff}$, and log g of stars from 13 photometric bands and *Gaia* DR2 parallaxes using a Mixture Density Network (MDN; Bishop 1994). A MDN is a neural network where the outputs parametrize a Gaussian mixture model:

$$p(\theta|x) = \Sigma_{j=1}^{n} \omega_j \mathcal{N}(\mu_j, \sigma_j) \tag{1}$$

Thus the outputs give a probability distribution function (PDF) and we use the negative log likelihood as our loss function. In other words, we train our network to maximize the sum of the log likelihoods of the output PDFs given the data. In this work, each of the MDNs we use have the same architecture. We use three fully connected layers with 32, 16 and 8 nodes. We apply a rectified linear function to each node as an activation function which makes the mapping from inputs to outputs highly non-linear.

3.2 Selecting Giant Stars

We first infer the log g and $T_{\rm eff}$ of all of the stars in our sample in order to select the giant stars. To do this, we train two MDNs using a random sample of 200,000 stars from the LAMOST DR3 catalog which pass our quality cuts (see Section 2.2). Both of these networks have one mixture component as the output so the inferred value is the mean of the Gaussian and the error is the width. We show a comparison of our derived values with the LAMOST results for 900,000 test stars in Figure 1. On average, our photometric $T_{\rm eff}$ values are lsmaller by 20 K with a standard deviation of 194 K.

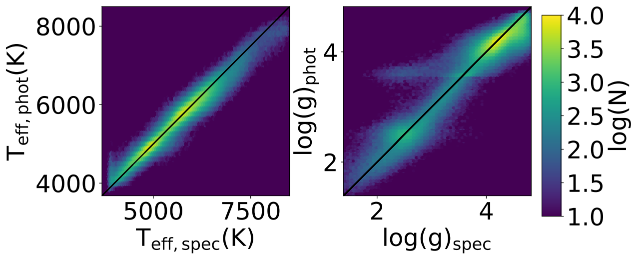

Figure 1. The stellar parameters (T_{eff} and log g) we derive from the photometry compared to the spectroscopically derived values from LAMOST. The mean difference between the T_{eff} is 20 K with a standard deviation of 194 K. The mean error in T_{eff} is 185 K with a standard deviation 444 K. The mean difference between the log g is .03 dex with a standard deviation of .27 dex. The mean log g error is 0.15 dex with a standard deviation of .07 dex. There is a group of stars that have spectroscopically derived log g <3.5 dex, and our derived values are > 3.5 dex. These stars generally have parallax errors > 0.05 mas. We only use these derived parameters to select giant stars and do not report them. These results are sufficient to select giant stars, however we are biased against stars with parallax errors > 0.05 mas.

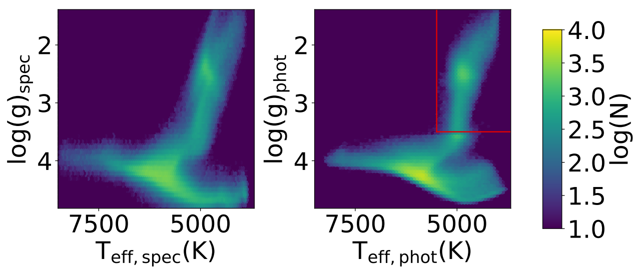

Figure 2. On the left is the LAMOST Kiel diagram for the testing sample and on the right is the photometric Kiel diagram. It is clear that the main sequence and giant branch are preserved in the photometric diagram. Therefore we can confidently select giant stars using these parameters. The red box in the photometric Kiel diagram (right) shows our selection.

The mean error on T_{eff} is 185 K with a standard deviation of 444 K. We also find the our photometric log g values are on average 0.03 dex smaller than the LAMOST values with a standard deviation of 0.37 dex. The mean log g error is 0.15 dex with a standard deviation of 0.07 dex. After inferring on all of the data that passes our quality cuts (see Section 2.1), we select stars with inferred log g < 3.5 dex and 2500 K < T_{eff} <5500 K as giant stars. How this selection looks with our test data is shown in Figure 2.

3.3 Selecting Red Clump Stars

We make our selection of red clump stars using inferred log g, T_{eff}, $\Delta\nu$ and ΔP. For each of these parameters we train another MDN. For T_{eff} and log g our network is trained on a subset of 200,000 giants stars selected using the method described in Section 3.2. Again we use one mixture component as the output so the inferred value is the mean of the Gaussian and the error is the width. In Figure 3, we show that we can accurately derive the stellar parameters from the photometry. On average our photometric log g values are 0.02 dex greater than the values from LAMOST with a standard deviation of 0.32 dex. The average error is 0.20 dex with a standard deviation of 0.10 dex. Our photometric T_{eff}values are larger than the LAMOST values by K on average with a standard deviation of 160 K, The average T_{eff} error is 3054 K with a standard deviation of 911,967 K. For $\Delta\nu$ and ΔP, we train on a subset of 30,000 stars from the sample presented in Ting et al. (2018). For the $\Delta\nu$ the network also has one mixture component as the output and we infer using the same method as T_{eff} and log gThe distribution of ΔP is bi-modal (see Figure 4). Using two mixture components helps the network to learn to reproduce this bi-modality. Therefore, the output of the ΔP network is a two component Gaussian mixture model. Our inferred ΔP is the weighted mean of the means of the two components and the error is the weighted mean of the widths of the two components. As the ΔP and $\Delta\nu$ signal in the photometry is weak, it is difficult to derive these parameters from the SED. However, we do remarkably well (see Figure 3). On average our derived $\Delta\nu$values are only 0.06 μHz less than the values derived from the LAMOST spectra in Ting et al. (2018) with a standard deviation of 1.75 μHz. The average error is 1.23 μHz with a standard deviation of 0.74 μHz. For ΔP, we find our values are, on average, -2 s smaller than the values derived in Ting et al. (2018) with a standard deviation of 75 s. The average error is 35 s with a standard deviation of 8.79 s.

To find the ideal red clump selection criteria, we look at the true positive rate and the contamination as a function of T_{eff}, log g, $\Delta\nu$ and ΔP. We bin our testing data using the inferred parameters and calculate the contamination and true positive rate within each bin. Although this is done in four dimensions (T_{eff}, log g, $\Delta\nu$ and ΔP), we show flattened two dimensional examples in Figure 5. We include bins with a low contamination while also having a significant percentage of the true red clump stars. Further information about the final sample can be found in Section 4.1.

3.4 Deriving Distances

Once we have our red clump sample, we infer the distances using the AllWISE W1 band similar to Ting & Rix (2019). First, we perform an extinction correction using the G−W1 color and A_G/A_{W1}=16 (Hawkins et al. 2017). Next, we use the less extincted stars to derive a relationship between the inferred T_{eff} and M_{W1}. Finally, we derive the distance using the distance modulus with the inferred M_{W1} and the extincted corrected W1 magnitudes.

4 RESULTS AND DISCUSSION

4.1 Red Clump Sample

In choosing our red clump sample, we prioritize a low contamination over a complete sample. To choose which bins from Figure 5 we will use in the final selection, we perform a cumulative summation sorted by the contamination rate. The results of this are shown in Figure 6. However, these

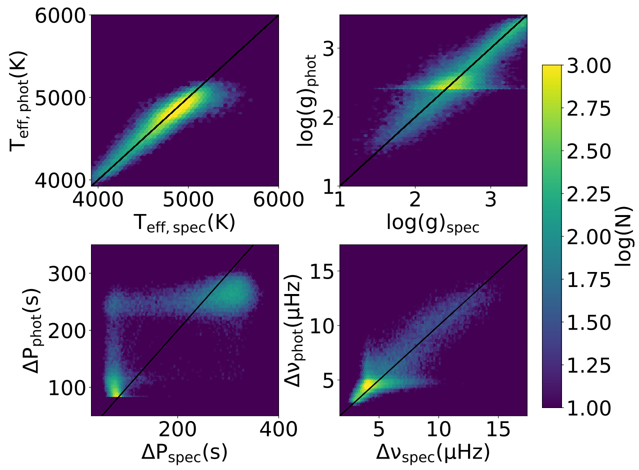

Figure 3. The stellar parameters ($T_{\rm eff}$, log g, ΔP and $\Delta\nu$) we derive for giant stars compared to the spectroscopically derived values from LAMOST and Ting et al. (2018). The mean difference between the $T_{\rm eff}$ is 24 K with a standard deviation of 160 K. The mean difference between the log g is 0.02 dex with a standard deviation of 0.32 dex. The mean difference between the ΔP is -3 s with a standard deviation of 75 s and the mean difference between the $\Delta\nu$ is -0.06 μHz with a standard deviation of 1.75 μHz. The ΔP is the most effective parameter for selecting red clump stars and the most difficult to derive from the photometry. From this figure we can see we are effective at picking up all of the red clump stars as the bottom right corner of the ΔP is empty. However, we do suffer from contamination in the top left corner. However, combining the ΔP with the other parameters can help limit this contamination.

results are a slight idealized. The selection method to create Figure 6 jumps around in the parameters space to selects the bins with the lowest contamination rate. For ease of selection, if we choose to only use adjacent bins we achieve a contamination rate of ∼25 % and a true positive percentage of ∼48%. These results are achieved by selecting stars with 4750 K < $T_{\rm eff}$ $\Delta\nu$ <5.5 μHz, and ΔP > 250 s.

4.2 Milky Way Map

In Figure 7 we show a preliminary map of the Milky Way made with red clump stars. To make this map we use the giant catalog from Poggio et al. (2018). This catalog does not include any data with Galactic longitude 300 deg. <l <360 deg. or Galactic latitude, |b| > 20 deg. It also only includes stars with *Gaia* G <15.5 mag. This catalog contains ∼ million giant stars. After applying our selection method, we find a catalog of ∼ 700,000 red clump stars with which we derive distances and make a Milky Way map.

5 SUMMARY

Red clump stars are standard candles proven to give more accurate distance measurements than parallaxes at distances > 3 kpc (Ting et al. 2018). However, identifying large pristine samples of red clump stars has historically been difficult. Red giant branch stars can have the same $T_{\rm eff}$ and log g making it easy to mistake them as red clump stars. The asteroseismic parameters ΔP and $\Delta\nu$ clearly separate helium core-burning red clump stars from inert core red giant branch stars (Bedding et al. 2011; Mosser et al. 2011; Stello et al. 2013; Mosser et al. 2014). These parameters have only been derived for ∼2,000 giant stars given the difficulty of the measurement and the amount of time required for light curve observations. Recently, Hawkins et al. (2018) demonstrated that the ΔP and $\Delta\nu$ can be derived from stellar spectra. Specifically, red clump stars can be selected from the difference in the carbon to nitrogen ratio due to mixing that occurs at the top of the red giant branch. In this work, we select red clump stars from the ∼ 400 million stars which have photometry from 2MASS, AllWISE, *Gaia*, and Pan-STARRS. We derive the $T_{\rm eff}$, log g, $\Delta\nu$, and ΔPof these stars from 13 bands of photometry and parallax using a mixed density network. We achieve a contamination rate of ∼25% when we select stars with $T_{\rm eff}$ > 4700 K, $\Delta\nu$ < 5μHz, and ΔP > 250 s. We apply our selection method to the giant catalog from Poggio et al. (2018). From the ∼600 million giant stars, we end with a red clump sample of ∼700,00 stars with which we make a Milky Way map. The next step is to apply our selection method to the entire sample of ∼ 400 million stars. Although spectroscopic methods provide a more pristine sample Hawkins et al. (2018); Ting et al. (2018), the photometric sample is much larger and contains more distant stars. For example, the LAMOST red clump sample from Ting et al. (2018) has 70% of the stars within 3 kpc and does not reach into the Galactic center or the outer Galactic halo. We expect our sample to precisely map the bulge and the outer halo. Given that distances are an essential but difficult measurement to make in Galactic archaeology, this map is sure to be used in many future studies of the formation and evolution of the Milky Way.

ACKNOWLEDGEMENTS

This work was initiated as a project for the Kavli Summer Program in Astrophysics held at the University of California – Santa Cruz (UCSC) in 2019. The program was co-funded by the Kavli Foundation, the National Science Foundation and UCSC. We thank them for their generous support.

This work has made use of data from the European Space Agency (ESA) mission *Gaia* (`https://www.cosmos.esa.int/gaia`), processed by the *Gaia* Data Processing and Analysis Consortium (DPAC, `https://www.cosmos.esa.int/web/gaia/dpac/consortium`). Funding for the DPAC has been provided by national institutions, in particular the institutions participating in the *Gaia* Multilateral Agreement.

This publication makes use of data products from the Two Micron All Sky Survey, which is a joint project of the University of Massachusetts and the Infrared Processing and Analysis Center/California Institute of Technology, funded by the National Aeronautics and Space Administration and the National Science Foundation.

The Pan-STARRS1 Surveys (PS1) have been made possible through contributions of the Institute for Astronomy, the University of Hawaii, the Pan-STARRS Project Office, the Max-Planck Society and its participating institutes, the Max Planck Institute for Astronomy, Heidelberg and the Max Planck Institute for Extraterrestrial Physics, Garching, The Johns Hopkins University, Durham University, the University of Edinburgh, Queen's University Belfast, the Harvard-Smithsonian Center for Astrophysics,

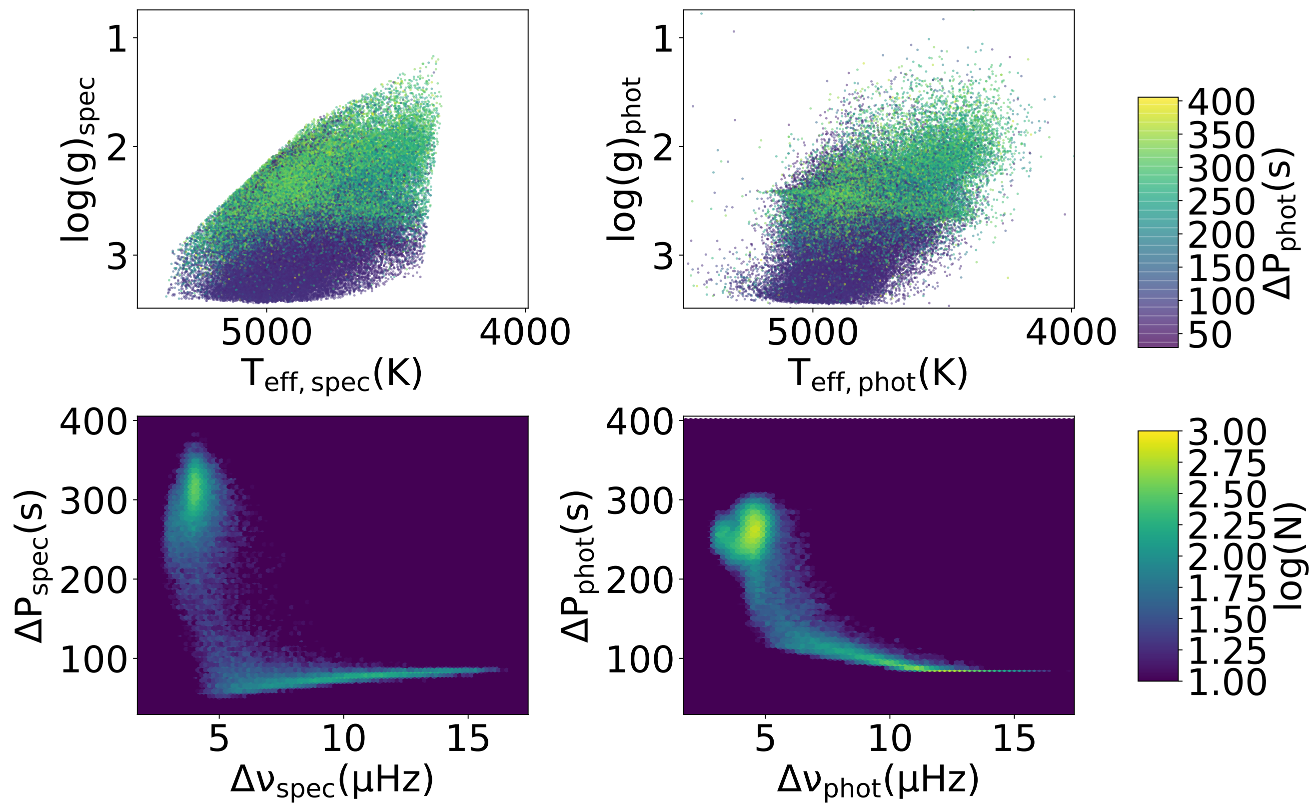

Figure 4. On the top left is the spectroscopic Kiel diagram of the convex hull from Ting et al. (2018) made and on the top right is the same stars with our photometrically derived parameters. Both plots are colored by the ΔP derived from spectra in Ting et al. (2018). It is clear that red clump stars (ΔP $>$ 200s) are more concentrated in certain regions of the parameter space. On the bottom left we show the asteroseismic parameters (ΔP and $\Delta\nu$) derived from LAMOST spectra in Ting et al. (2018). On the bottom right we show our derived asteroseismic parameters. It is clear we can still pick out the red clump with ΔP $>$ 200 s.

the Las Cumbres Observatory Global Telescope Network Incorporated, the National Central University of Taiwan, the Space Telescope Science Institute, the National Aeronautics and Space Administration under Grant No. NNX08AR22G issued through the Planetary Science Division of the NASA Science Mission Directorate, the National Science Foundation under Grant No. AST-1238877, the University of Maryland, and Eotvos Lorand University (ELTE).

REFERENCES

Arenou F., et al., 2018, A&A, 616, A17
Beck P. G., et al., 2011, Science, 332, 205
Bedding T. R., et al., 2011, Nature, 471, 608
Bishop C. M., 1994, Technical report, Mixture density networks
Bovy J., et al., 2014, ApJ, 790, 127
Casey A. R., Hogg D. W., Ness M., Rix H.-W., Ho A. Q., Gilmore G., 2016, ArXiv e-prints:1603.03040,
Castellani V., Chieffi A., Straniero O., 1992, ApJS, 78, 517
Chambers K. C., et al., 2016, arXiv e-prints, p. arXiv:1612.05560
Chaplin W. J., Miglio A., 2013, ARA&A, 51, 353
Evans D. W., et al., 2018, A&A, 616, A4
Gaia Collaboration et al., 2016, A&A, 595, A1
Gaia Collaboration et al., 2018, A&A, 616, A1
Girardi L., 2016, ARA&A, 54, 95
Hawkins K., Leistedt B., Bovy J., Hogg D. W., 2017, MNRAS, 471, 722
Hawkins K., Ting Y.-S., Walter-Rix H., 2018, ApJ, 853, 20
Mainzer A., et al., 2011, ApJ, 743, 156
Majewski S. R., et al., 2015, ArXiv e-prints:1509.05420,
Marrese P. M., Marinoni S., Fabrizio M., Altavilla G., 2019, A&A, 621, A144
Martell S. L., Smith G. H., Briley M. M., 2008, AJ, 136, 2522
Masseron T., Gilmore G., 2015, MNRAS, 453, 1855
Masseron T., Hawkins K., 2017, A&A, 597, L3
Masseron T., Lagarde N., Miglio A., Elsworth Y., Gilmore G., 2017, MNRAS, 464, 3021
Miglio A., et al., 2009, A&A, 503, L21
Mosser B., et al., 2010, A&A, 517, A22
Mosser B., et al., 2011, A&A, 532, A86
Mosser B., et al., 2014, A&A, 572, L5
Ness M., Hogg D. W., Rix H.-W., Ho A. Y. Q., Zasowski G., 2015, ApJ, 808, 16
Poggio E., et al., 2018, MNRAS, 481, L21
Skrutskie M. F., et al., 2006, AJ, 131, 1163
Stanek K. Z., Udalski A., SzymaŃski M., KaŁuŻny J., Kubiak Z. M., Mateo M., KrzemiŃski W., 1997, ApJ, 477, 163
Stanek K. Z., Zaritsky D., Harris J., 1998, ApJ, 500, L141
Stello D., et al., 2013, ApJ, 765, L41
Taylor M. B., 2005, in Shopbell P., Britton M., Ebert R., eds, Astronomical Society of the Pacific Conference Series Vol. 347, Astronomical Data Analysis Software and Systems XIV. p. 29
Ting Y.-S., Rix H.-W., 2019, ApJ, 878, 21
Ting Y.-S., Hawkins K., Rix H.-W., 2018, ApJ, 858, L7
Wright E. L., et al., 2010, AJ, 140, 1868

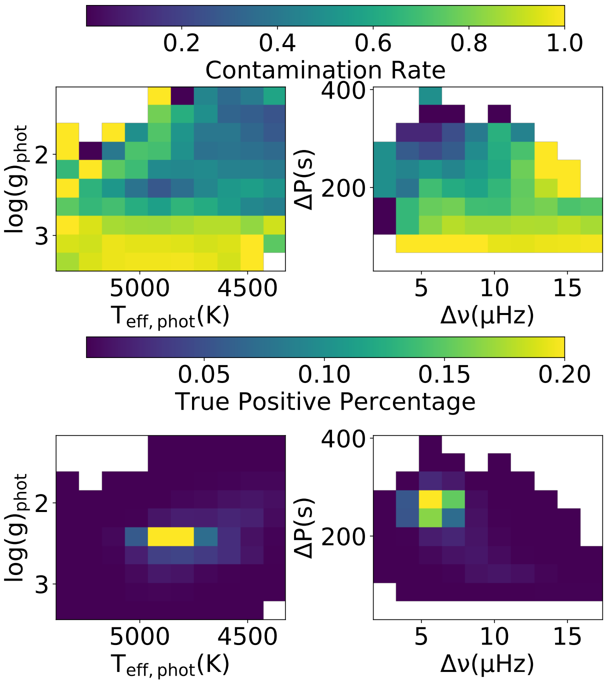

Figure 5. The top plot shows the contamination rate in different in T_{eff} and $\log g$(left) as well as $\Delta\nu$ and ΔP (right) bins. This contamination rate is calculated by selecting everything within the bin as red clump and finding what percentage of them are false positives using the Ting et al. (2018) as the ground truth. The bottom plots show what percentage of the true positives are in each bin. We can use this binning to optimize the selection in all four parameters in order to simultaneously minimize the contamination rate and maximize the true positive percentage.

Xiang M.-S., et al., 2017, MNRAS, 467, 1890

This paper has been typeset from a TEX/LATEX file prepared by the author.

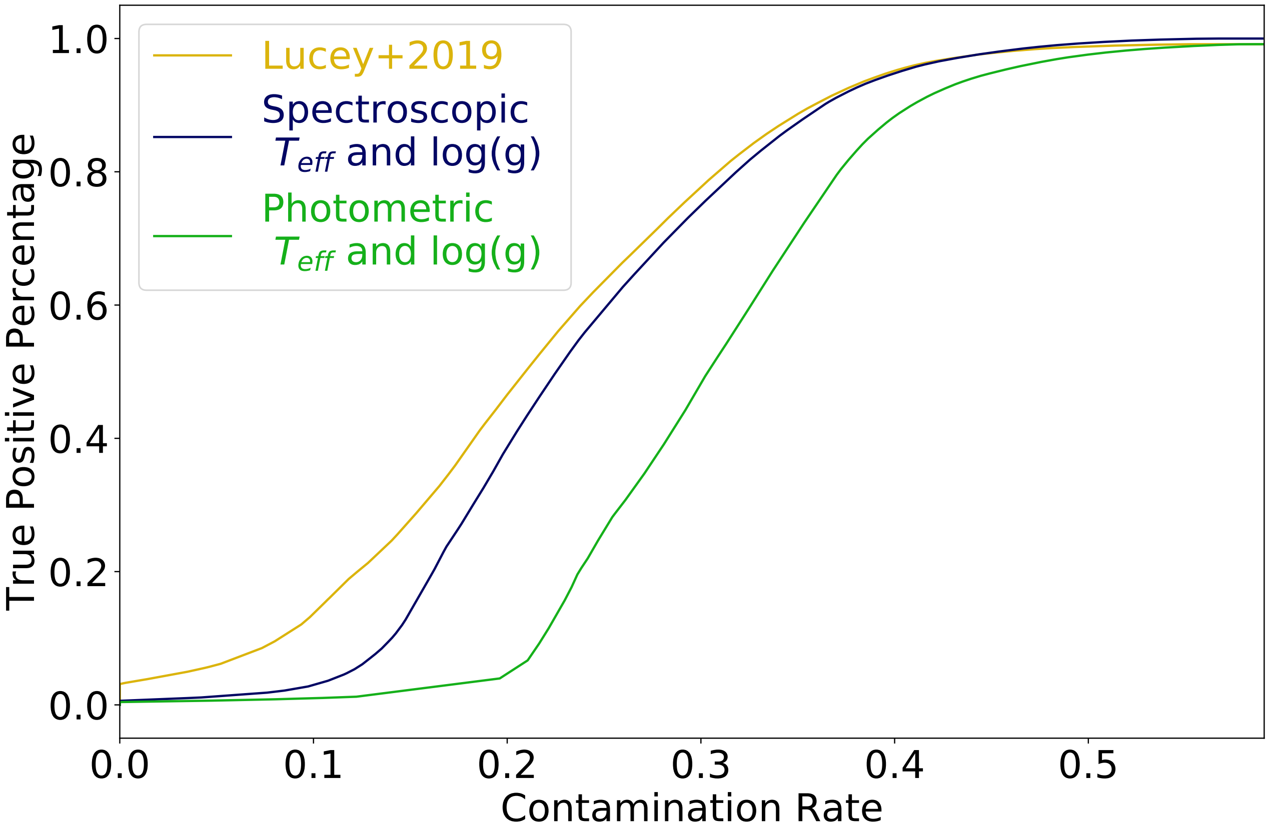

Figure 6. The accuracy of our selection method compared to other methods. The lines are calculated by cumulatively summing bins like those shown in Figure 5. The result for our method where we bin in all four photometrically derived parameters (T_{eff}, log g, $\Delta\nu$, and ΔP) is shown in yellow. The result of only selecting in the photometric T_{eff} and log g space is shown in green. The results of making the same selection but using spectroscopically derived T_{eff} and log g is shown in blue. This shows our method is the most accurate. We can obtain a higher true positive percentage for a given contamination rate than the other two methods. The spectroscopic parameter selection is more accurate because the precision and accuracy of the parameters is higher than the photometric parameters.

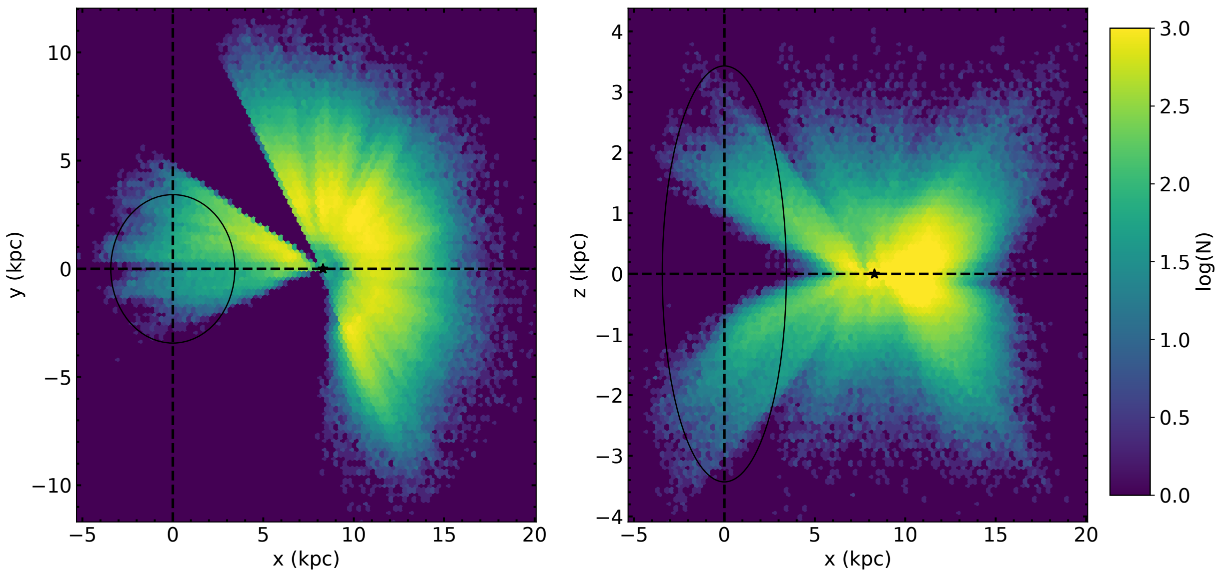

Figure 7. Map of the Milky Way made with giant stars from Poggio et al. (2018). On the left is the density of stars in Galactic coordinates, X and Y and on the right are the Galactic coordinates X and Z. The Galactic center is located at (0,0,0) in both plots and the Sun is located at (8.3,0,0). The catalog from Poggio et al. (2018) does not include any stars out of the Galactic plane ($|b| > 20$ deg) and does not include an stars with 300 deg $< l <$ 330 deg. This map will be improved when we use our own giant catalog. It will reach far into the halo and deeper into the Galactic center.